Chapter

Effects of Electron Irradiation on Optical Properties of Bismuth-Doped Phosphosilicate Fiber

Alexander V. Kir'yanov and Arindam Halder

Abstract

The basic optical properties of yttrium-phosphosilicate fiber doped with bismuth (Bi) are assessed in both pristine state and that established after bombardment by a beam of high-energy electrons. The fiber has been developed and fabricated with a target to use it for laser applications in visible/near-infrared (VIS/NIR) domain. In this chapter, the main attention is paid to the dramatic changes in absorption spectra of the fiber under electron irradiation. Meanwhile, we reveal its overall resistance to irradiation in terms of emissive potential and bleaching contrast at excitation into the absorption bands of bismuth-related active centers. Besides, we report a new effect of large dose-dependent Stokes shift, experienced by the fiber's cutoff wavelength, which arises due to refractive index rise in its core area. The laws obeyed by the fiber's characteristics vs. dose are examined for possible applications in dosimetry.

Keywords: bismuth, yttrium-phosphosilicate fiber, electron irradiation, optical properties, cutoff wavelength

1. Introduction

Silica-based fibers doped with semi-metals, e.g., bismuth (Bi), have become a popular object for sensing ionizing radiation (dosimetry), including electron beams: recently some of the Bi-doped fibers (BDFs) were primarily examined in this regard [1–8]. Sensing dose of ionizing radiation using optical fiber is an important issue: dose-induced changes in its characteristics are worth assessing as they may serve a base for making cost-effective, remotely monitorable sensors, easily located in harsh environments such as proximity to a nuclear reactor [9]; optical fibers can be also used for plasma diagnostics in fusion reactors [10]. The relevance of choosing BDFs for sensing relies on the understanding that Bi is highly susceptible to interaction with nuclear particles, e.g., energetic (further "β") electrons. Since high-energy "primary" β-electrons are virtually non-dissipating at propagation through silica fiber, the basic effect behind the transformations arising in its material and optical properties is creating β-induced carriers, viz., "secondary" free holes/electrons. Given that Bi is a heavy semi-metal, it becomes—when used as dopant—a powerful source of secondary carriers, eventually stabilized in core glass network generating plenty of defect centers. Such centers (a part of which is associated with the presence of Bi ions) are

responsible for the increasing dose-dependent-induced absorption (IA) in BDFs and, accordingly, modifications of absorption and emission bands of Bi-related active centers (BACs). So far, BDFs with core glass of various chemical compositions were examined in this regard. Particularly, it was demonstrated that BDFs with aluminosilicate and germanosilicate hosts are highly susceptible to different types of ionizing radiations [1–8], with the result being notable growth of IA in visible/near-infrared (VIS/NIR) and severe changes in the absorption bands of the respective BACs. Say, it was found that Bi/Ge and Bi/Si BACs fade while Bi/Al BACs are born posterior to β-irradiation. However, the case of Bi-doped phosphosilicate fiber remained untouched.

In this chapter, we present a review of our recent studies of the basic material and optical properties of a homemade Bi-doped yttrium-phosphosilicate (BYP) fiber in pristine state [11–13] and after irradiating by a beam of β-electrons [14]. The review's main scopes are dose-induced transformations in absorptive, emissive, and waveguide characteristics of the fiber. The data presented below can serve a base for its use for dosimetry purposes.

2. Optical properties of BYP fiber in pristine state

BYP fiber (its cleaved-end image is shown in **Figure 1**) was drawn from the preform, fabricated by employing modified chemical vapor deposition process along with solution-doping techniques; the details are reported in [11, 12].

The basic characteristics of BYP fiber are summarized in **Table 1**.

The cross-sectional distributions of the doping elements (P, Y, and Bi) within the core region of BYP preform were measured using electron microprobe analysis and are plotted in **Figure 2**; their contents were found to be 5.26, 0.14, and 0.07 wt.%, respectively.

The basic waveguide properties of the fiber, viz., numerical aperture (NA), ~0.11; core diameter, ~4.42 μm; and refractive-index (RI) difference, ~0.004, were managed to fulfill single-mode propagation of light beyond ~600 nm, which is potentially perspective for amplifying/lasing in VIS/NIR [13].

The RI transversal distribution of BYP fiber was obtained using a fiber profilometer and is shown in **Figure 3**.

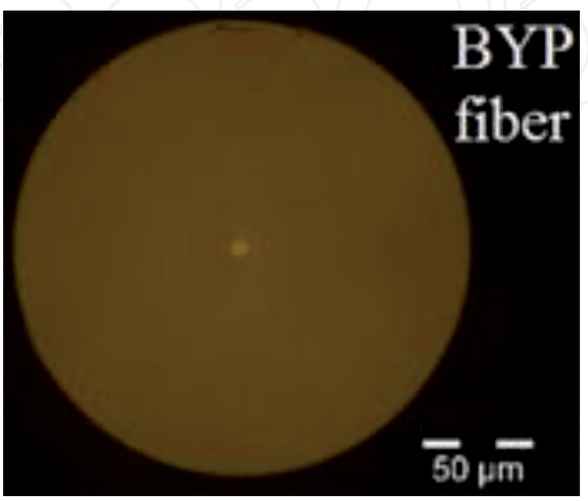

Figure 1.
Cross-sectional image of BYP fiber.

	Dopants' concentrations (wt.%)	Core/cladding diameters (μm)	NA	Cutoff wavelength (nm)
BYP fiber	P = 5.26 Y = 0.14 Bi = 0.07	4.4/123.3	0.12	645

Table 1.
Optical properties of BYP fiber.

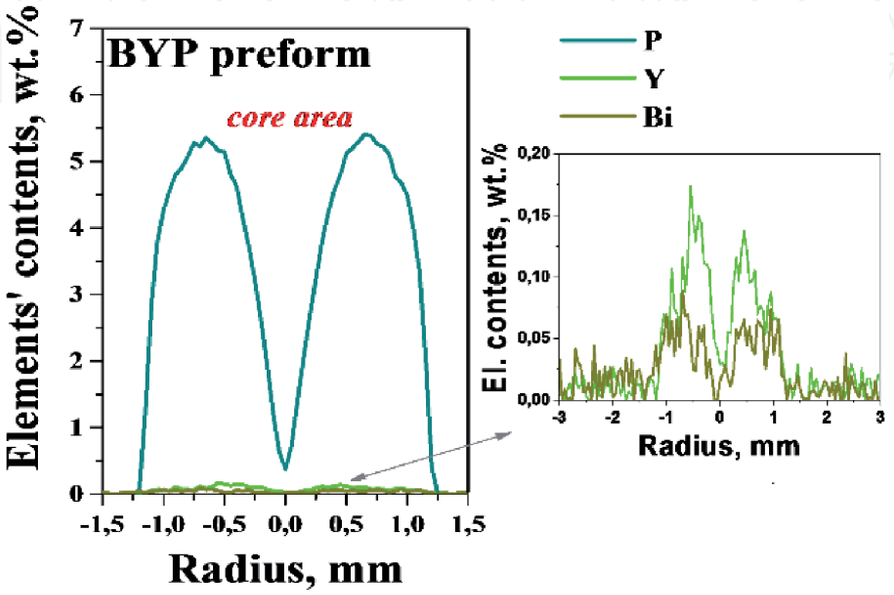

Figure 2.
Cross-sectional distributions of the dopants in BYP fiber preform.

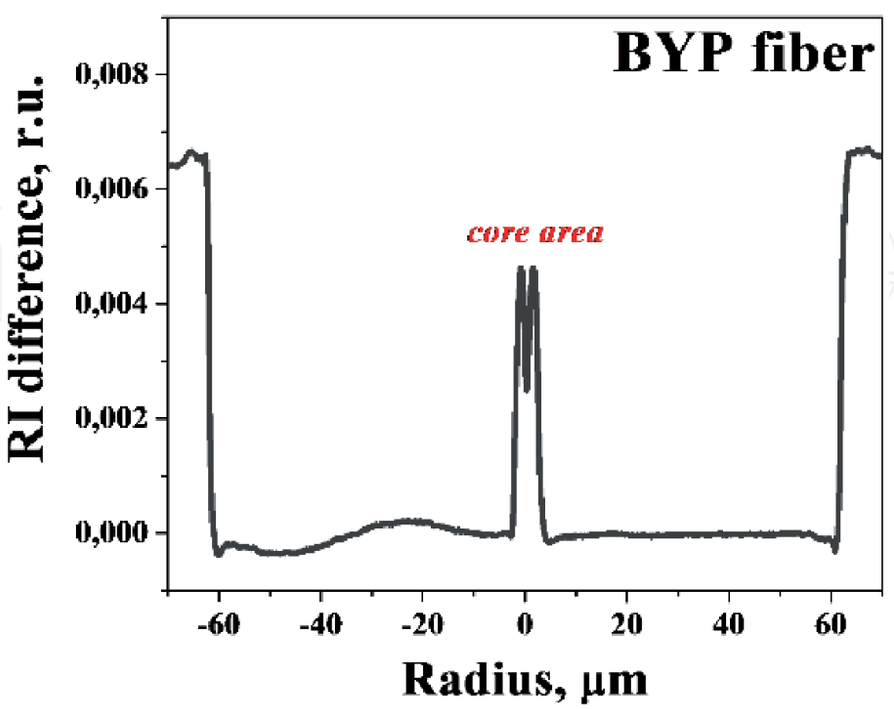

Figure 3.
RI profile of BYP fiber.

The fiber's spectral attenuations in straight and coiled positions were measured, and their difference was found; the result is shown in **Figure 4**. As seen from the figure, the stop wavelength of spectral oscillations is at ~645 nm (in fact, it is the cutoff wavelength λ_c), beyond which the fiber supports single-mode propagation ($LP_{0,1}$ mode).

The absorption, or loss, spectrum $\alpha_0(\lambda)$ of BYP fiber (the solid line in **Figure 5**) was measured using a white-light (WL) source with fiber output and optical spectrum analyzer (OSA) by the cutback method. As seen, the main spectral features of its spectral attenuation (i.e., the broad absorptions bands in VIS/NIR) match the ones known for Bi-related (Bi/P and Bi/Si) BACs. As also seen from the figure, these bands are superimposed with the background (base) loss, steadily growing toward shorter wavelengths, a well-known feature for BDFs. This background loss was recently shown to be explained by Rayleigh scattering (RS) on Bi nanoparticles in the core region [12]; see the dashed line in **Figure 5**.

Photoluminescence (PL) spectra of BYP fiber were recorded in "forward" geometry at in-core pumping using a set of low-power laser diodes (LDs) with fiber outputs. The pump wavelengths explored were 405, 520, 633, 720, 905, and 976 nm (see the arrows in **Figure 5**, the colors of which are congruent with the spectral subdomains where excitation lights fall in). Lengths (L_f) of fiber samples were chosen to provide comparable optical densities (OD = $\alpha_0 L_f$) at these wavelengths, in accord with spectrally variable extinction in the BAC bands. Note that OD was chosen to be ~2.5, providing effective pump absorption and, in the meantime, a little effect of PL reabsorption. The resultant PL spectra are shown in **Figure 6**, all recorded at the same incidence power at each pump wavelength (~3.5 mW). Such pump level was chosen, on the one hand, to provide population inversion in the system of BACs sufficient to get pronounced PL power and, on the other hand, to guarantee safety of registration with OSA. As seen, BYP fiber demonstrates pronounced PL in VIS/NIR, characteristic to BACs in phosphosilicate fibers [1, 11–13],

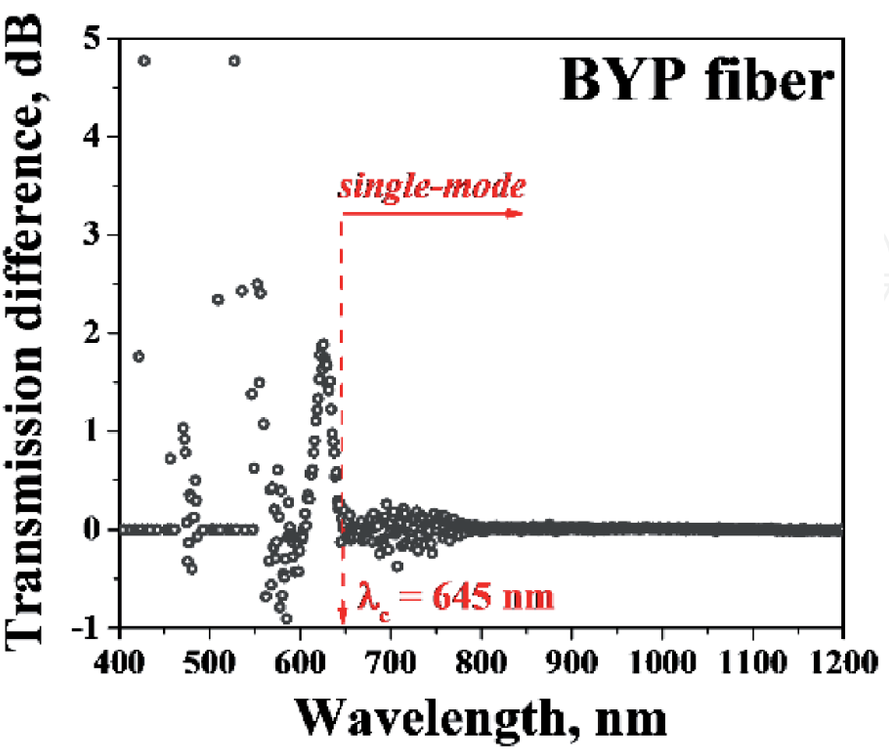

Figure 4.
Transmission difference (straight to coiled positions) of BYP fiber, revealing the spectral position of the cutoff wavelength (~645 nm).

with maximum at ~1200–1300 nm slightly depending on the excitation wavelength. Say, when pumped at 405 nm, BYP fiber demonstrates the PL bands centered at 760 and 1280 nm. In turn, when pumped in NIR (at 730 and 905 nm), it emits the second band only, whose gravity center is barely shifting to shorter wavelengths with increasing pump wavelength.

The behavior of nonlinear, viz., in function of pump power P_{in}, absorption, or loss, of BYP fiber, parametrized for the same set of pump wavelengths, is illustrated in **Figure 7**. Experimentally, pump light from a LD was launched through splice to a fiber sample with length L_f (chosen as reciprocal of α_0; hence, L_f were different for each kind of excitation). Its nonlinear transmission was measured as $T_{NL} = P_{out}/P_{in}$ (where P_{in} and P_{out} are the input and output pump powers, respectively), and nonlinear absorption (loss) was then found as $\alpha_{NL} = -10\log(T_{NL})/L_f$. The dependences α_{NL} *vs*. P_{in}, obtained for different pump wavelengths, are plotted in **Figure 7**.

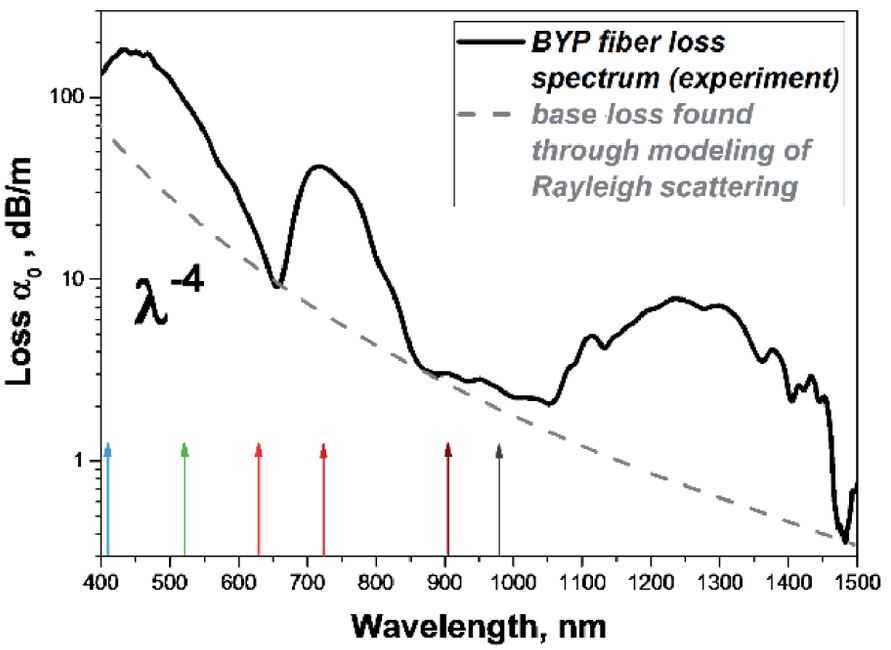

Figure 5.
Experimental absorption spectrum of BYP fiber (solid line) and modeled RS loss spectrum. The excitation wavelengths used in the experiments are marked by arrows of different colors.

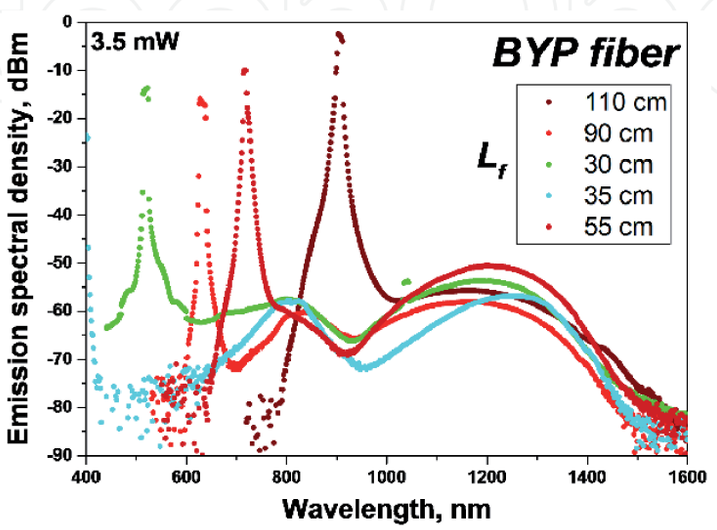

Figure 6.
PL spectra at BYP fiber's output, obtained at different excitation wavelengths (405, 520, 633, 720, and 905 nm); lengths of fiber pieces used are given in the inset.

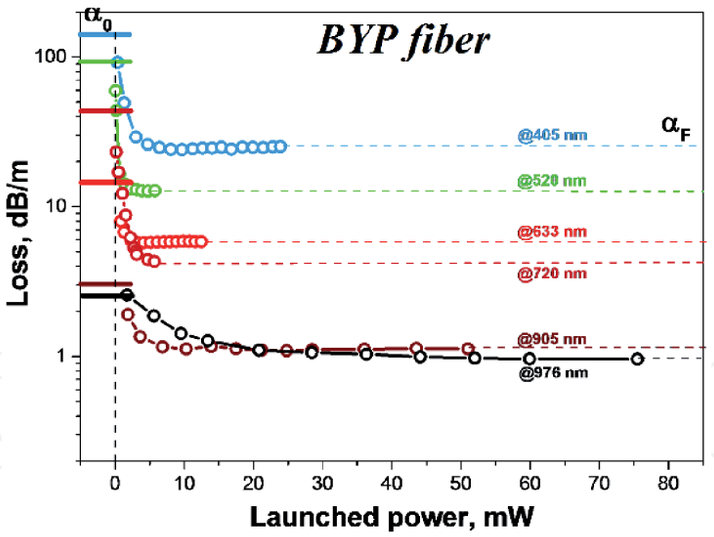

Figure 7.
Dependences of nonlinear loss α_{NL} vs. launched pump power Pin *in BYP fiber, built for all excitation wavelengths (highlighted by relevant colors). The small-signal absorptions (αo) at these wavelengths were found from* ***Figure 5****. The residual losses (αF) are marked by the dashed lines.*

Note that the plateaus (marked as α_F in the figure), to which the dependences approach at higher pump powers, attribute the unbleached, or residual, absorptions. As seen, for the shorter wavelengths, the loss plateaus (α_F-values) lie above those for the longer ones.

Unbleached loss in the BYP fiber might arise in the system of BACs due to a line of processes such as excited-state absorption (ESA), up-conversion in clustered BACs, scattering on nano-inclusions, etc., thanks to a "cumulative" effect of the mentioned contributions. Generally, it is difficult to undoubtedly segregate the true origin of the effect. Meanwhile, as demonstrated in [12] for the BDFs invented by our team, RS loss may stand behind the phenomenon. For example, for BYP fiber, if the residual losses α_F are plotted in double logarithmic scale vs. excitation wavenumber (reciprocal of wavelength λ: $10^4/\lambda$), the data obey the $\sim\lambda^{-4}$ law with high accuracy. This points on that RS can be a good explanation for growth of the residual (unbleached) loss with decreasing wavelength, $\alpha_F(\lambda)$.

3. Optical properties of BYP fiber after electron irradiation

A controllable linear accelerator emitting β-electrons with a narrow-band energy spectrum (~6 MeV) in a short-pulse (~5-μs) mode was used for irradiating BYP fiber [1]. Its samples ~2 m in length were placed inside the accelerator's chamber for the growing fluence of β-irradiation. Prior to optical measurements, the irradiated samples were relaxed for a month at room temperature to minimize the role of short-decay components in IA; for the same reason, the measurements were done during the following short period of time (2–3 weeks). Five irradiation fluxes (doses) ("1" to "5") were chosen to exemplify the type of changes in optical properties of the fiber, established after β-bombardment: 3×10^{11}, 1×10^{12}, 3×10^{12}, 1×10^{13}, and 1×10^{14} cm^{-2} [69, 230, 6.9×10^2, 2.3×10^3, and 2.3×10^4 $Gy(SiO_2)$]; its pristine state is referred to as "0" [14].

The basic trends in dose-related modifications of the optical properties of BYP fiber can be captured from **Figures 8–15**.

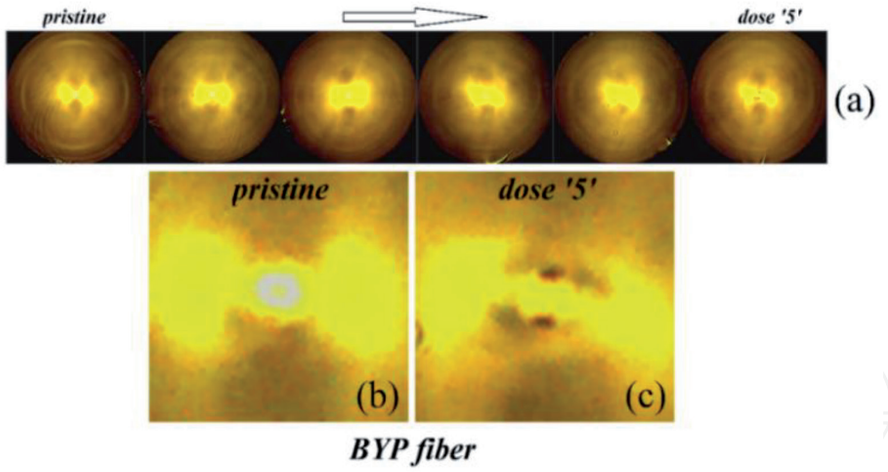

Figure 8.
(a) Cross-sectional images of BYP fiber, obtained for different irradiation doses; the arrow highlights dose increasing. (b and c) insights to core region for BYP fiber in pristine state and after experiencing maximal irradiation dose ("5"), respectively.

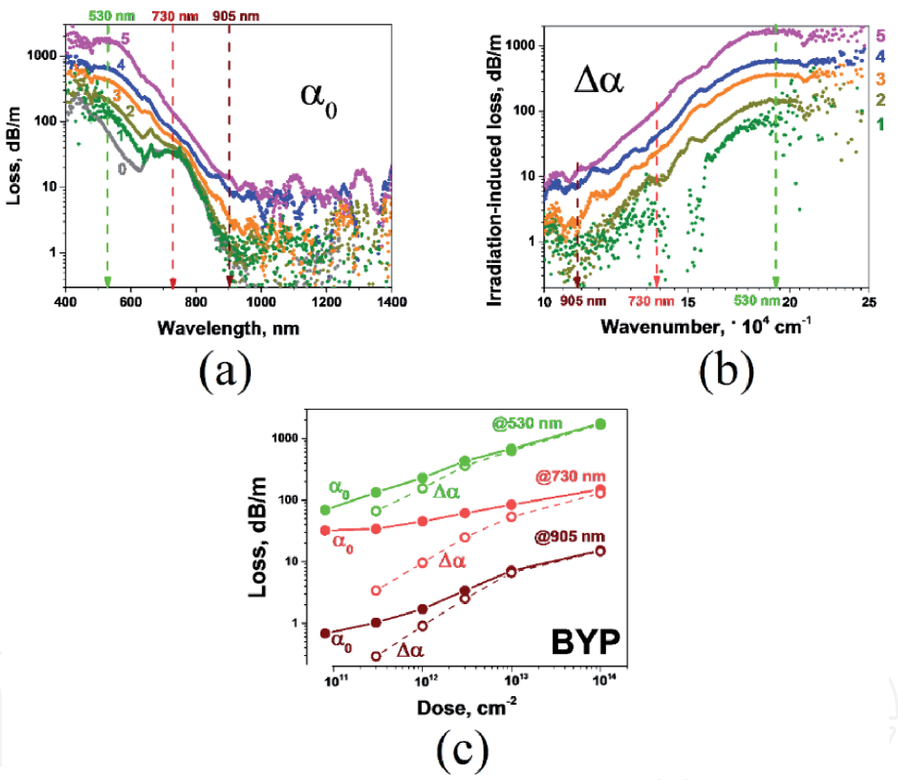

Figure 9.
(a) Attenuation spectra (α0) in VIS/NIR vs. wavelength and (b) IA spectra (Δα) vs. wavenumber for BYP fiber in pristine state (curves "0") and after growing β-irradiation dose (curves "1" to "5"). (c) Dose dependences of small-signal absorption (α0, solid curves) and IA (Δα, dashed curves), measured at wavelengths 905, 730, and 530 nm.

In **Figure 8**, we demonstrate how β-bombardment affects WL transmission of the fiber. It is seen that it suffers darkening (steadily increasing with growing irradiation dose) within the core area but its un-doped silica cladding is barely affected by irradiation.

In **Figure 9**, the absorption spectra vs. wavelength (a) and wavenumber (b) are shown, measured for BYP fiber in pristine state and after β-irradiation with doses 1 to 5 (curves "0" to "5"). As seen, IA magnitudes ($\Delta\alpha$) are very large in the fiber, especially in UV/VIS where IA reaches >2000 dB/m at maximal dose 5.

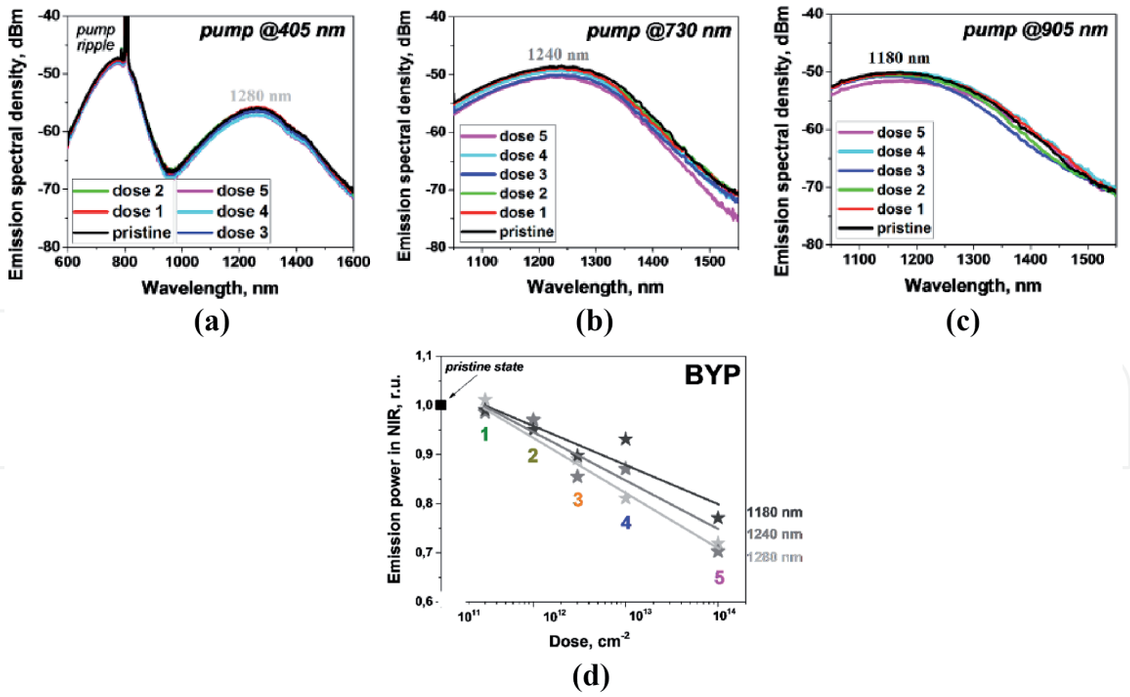

Figure 10.
(a–c) PL spectra of BYP fiber at optical excitation at 405 (a), 730 (b), and 905 (c) nm with launched powers ~25, ~20, and ~100 mW, respectively. (d) Dose dependences of relative (to pristine state) PL powers in the maxima of BAC bands shown in panels (a–c).

It is natural to ascribe the dramatic IA rise in BYP fiber to Bi/P co-doping (doping with Y plays a minor role as "light" Y atom is nearly irresponsible for creating defect centers by nuclear particles.) The spectrally dependent IA in the fiber can be explained likewise that in β-irradiated aluminosilicate BDFs [1, 2], its rise in VIS seemingly originates from extra Bi/P BACs generated, while its gravity center shift toward UV is related to growth of P-centers. Besides, possible contribution in the latter trend may stem from growth of RS (yet occurring in pristine BYP fiber; see [13]) due to irradiation-induced nanoscale degradation of core glass. However, given that IA spectra of irradiated BYP fiber are essentially structureless, it is nearly impossible to separate the evoked mechanisms. The dose-dependent trends for overall loss (α_0) and IA ($\Delta\alpha$), specified for wavelengths 530, 730, and 905 nm [see the dashed vertical lines in **Figure 9(a)** and **(b)**] are resumed in **Figure 9(c)**. Tentatively, the monotonic changes with the dose of both quantities are promising for dosimetry.

In **Figure 10(a)–(c)**, we exemplify the spectral transformations in BAC PL at pumping the fiber at 530, 730, and 905 nm for the growing dose of β-irradiation. In turn, we summarize in **Figure 10(d)** the dose-related changes in PL power. In this case, the same set of equipment and measurement techniques were employed as when studying pristine BYP fiber (refer to **Figure 6** and the text therein). As seen from **Figure 10**, the emissive potential of BYP fiber at either excitation wavelength decreases but barely with dose (not exceeding ~15% at the highest received dose 5, ~10^{14} cm^{-2}). Seemingly, this happens because of generating of extra emission-active Bi/P BACs during irradiation (like it happens with Bi/Al BACs in Bi-doped aluminosilicate fiber [1, 2]), a process leveling the deteriorating effect of IA growth on other defect centers. Thus, BYP fiber is quite resistant to β-irradiation, suggesting its usefulness for remote dosimetry, e.g., at a nuclear plant.

In **Figure 11**, we specify for BYP fiber the bleached part of absorption under pumping at different wavelengths [405 (a), 730 (b), and 905 (c) nm], parametrized

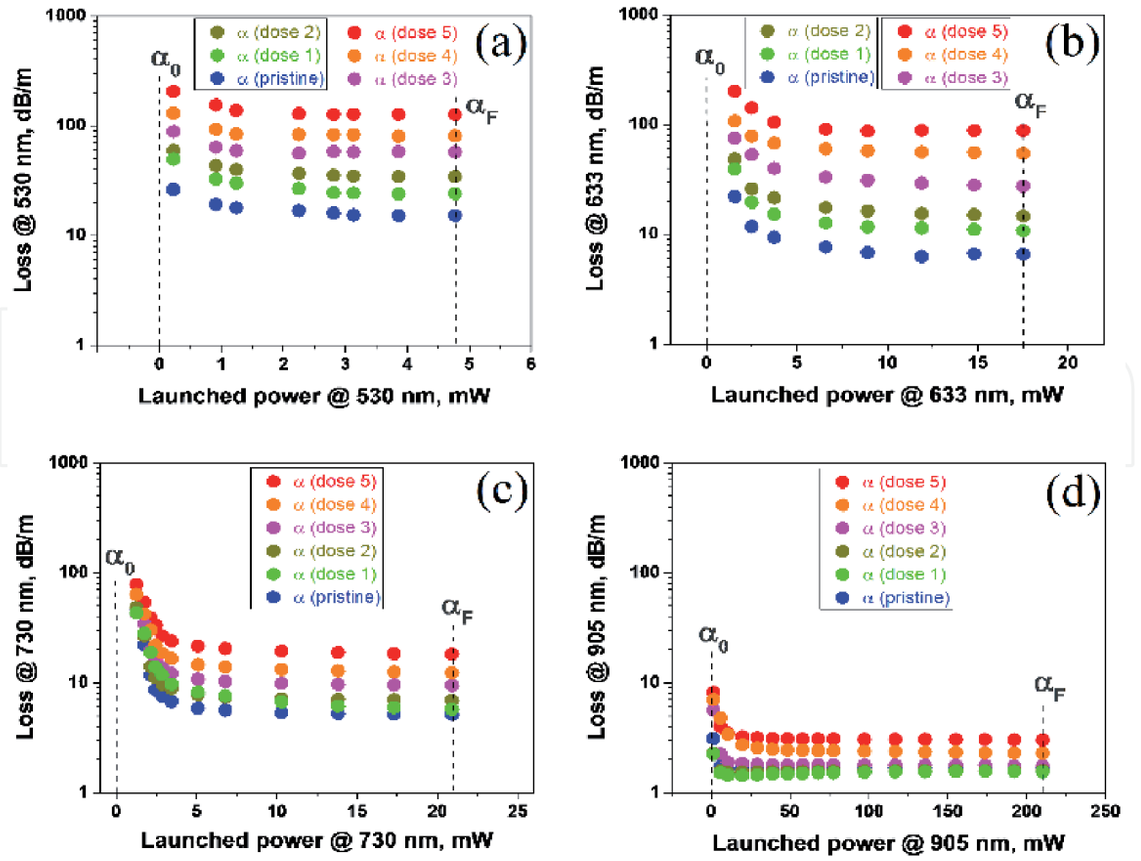

Figure 11.
Nonlinear absorption coefficients of BYP fiber in pristine state and after different doses of β-irradiation (curves 1 to 5) vs. launched LD pump power at 530 (a), 633 (b), 730 (c), and 905 (d) nm.

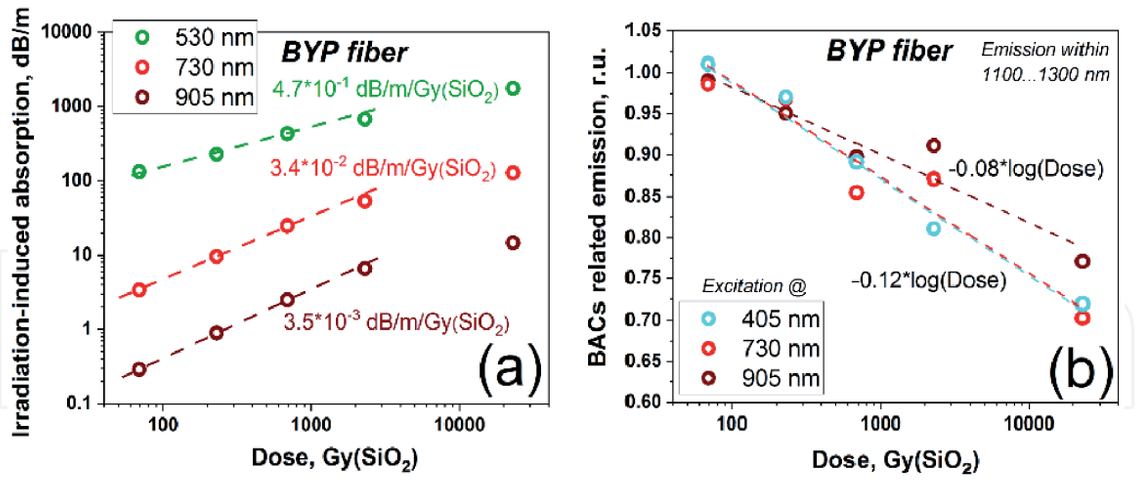

Figure 12.
Prospects for dosimetry using BYP fiber, based on (a) IA rise at 905, 730, and 530 nm and (b) Bi-related emission drop at excitations at 905, 730, and 405 nm vs. β-irradiation dose (symbols and dashed lines correspond to experimental data and their fits, respectively). The dose laws are provided near the experimental dependences: in (a) the slopes of the linearized fits within different spectral domains and in (b) the formula for fitting. All characteristics are given against dose in Gy[SiO$_2$].

for different irradiation doses (see the symbols of different colors in the panels). The experiments were done by the same way as described above for the pristine BYP fiber (see **Figure 7** and the text therein). As seen from **Figure 11**, all the dependences $\alpha_{NL}(P_{in})$, including the values of small-signal (α_0) and residual (α_F) losses for the wavelengths examined, are all shifted upward with increasing irradiation

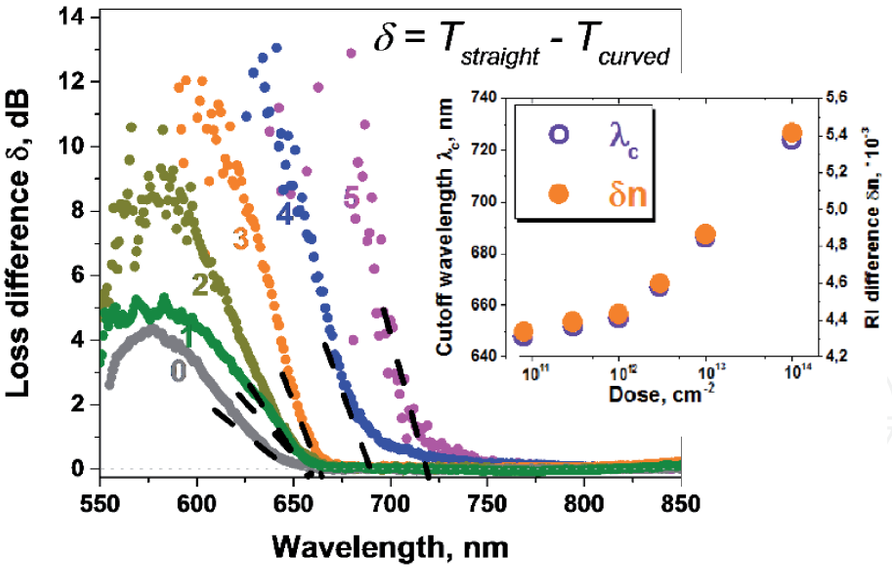

Figure 13.
Main frame: transmission difference spectra of BYP fiber in pristine state and after different irradiation doses, measured at arranging it straight and coiled (for diameter of 5 cm); the cutoff wavelengths λ_c are defined by intersections of the black dashed lines with the horizontal axis. Inset: dose dependences of cutoff wavelength λ_c (left axis, open violet circles, left axis) and RI difference δn *(right scale, orange-filled circles).*

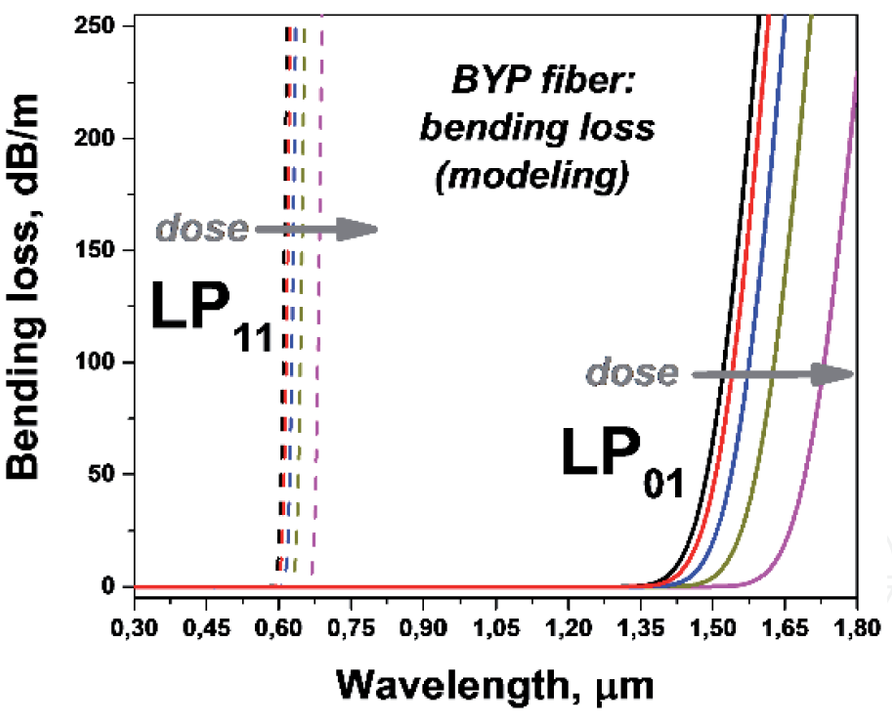

Figure 14.
Results of simulation of bending losses for LP_{01} and LP_{11} modes of BYP fiber bended for 30-cm diameter in pristine state and for the growing doses from 2 to 5 (the arrows highlight dose increasing).

dose; however, the longer the excitation wavelength, the effect is weaker. We suppose that the growth of unbleached loss α_F with dose is explained by boosted scattering in the system of BACs (see above) or/and by P_1-centers produced during irradiation [15, 16]. In the meantime, the growth of bleached part of absorption α_0 with dose arises due to generation of extra Bi/P BACs, which prevails that of residual loss α_F. This trend seems to be advantageous for laser applications of BYP fiber in harsh environments.

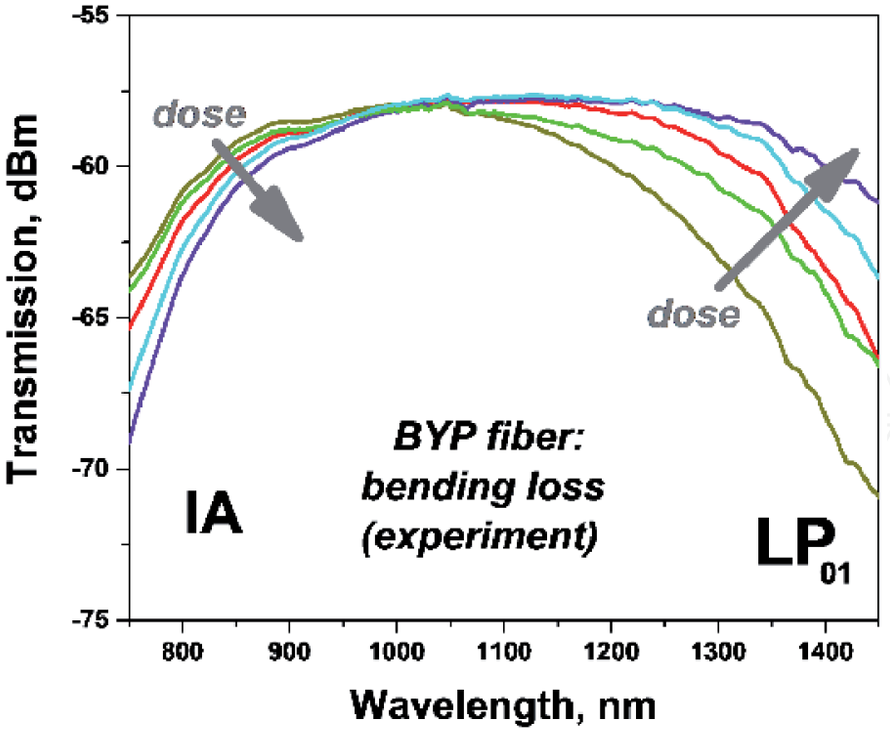

Figure 15.
Experimental transmission spectra of 12-cm BYP fiber samples, similarly bended, being in pristine state and for the growing doses from 2 to 5 (the arrows highlight dose increasing); the spectral ranges where dominate IA and partial escaping to cladding of LP_{01} mode are on the left and right, respectively.

In **Figure 12**, we provide a resume of the basic set of data (reported above) as a base for farther dosimetry assessments of BYP fibers. Note that here the changes in the characteristics under scope are related to irradiation dose counted in Gy[SiO_2] (instead of fluence in cm^{-2}), for comparison of some of them with those previously published for Bi,Y-free phosphosilicate fibers [17, 18].

Regarding the IA growth with dose in BYP fiber, it is seen from (a) that in *log–log* plot this quantity changes with dose up to ~5 kGy[SiO_2] by a nearly linear law but with slope reduced by approximately two orders of value from NIR to VIS. Notably, this trend in NIR range (where BAC absorption is less prominent than in VIS) is less expressed than that reported for un-doped phosphosilicate fiber exposed to X-rays in [17].

Regarding the reduction of NIR PL specific to BACs (within 1.1–1.3 μm) with dose, it is seen from (b) that it steadily diminishes with slope, slightly dependent upon pump wavelength used. The found law inherent to BYP fiber can be used for dosimetry for a wide interval of doses (tens Gy[SiO_2] to tens kGy[SiO_2]).

Another property of BYP fiber, viz., the character of modal wave guidance, was found to severely change with irradiation dose, too. In this regard, a new effect of large Stokes shift, experienced by cutoff wavelength of the fiber vs. dose, was uncovered; its main sides can be revealed from **Figures 13–15**.

Experimentally, we measured bending loss of BYP fiber at each stage of β-irradiation. Probing the fiber with WL, we found spectrally dependent losses in its pristine and irradiated (with different doses) states when it is placed straight and coiled (for ~5-cm diameter); then we found their difference. The resultant spectra are shown in the main frame of **Figure 13**. Note that the last to the Stokes side oscillations in the figure correspond to the first cutoff wavelengths (λ_c) of the fiber after its exposure to different doses (these are marked by the dashed black lines). Beyond these spectral points, only fundamental LP_{01} mode is guided in the fiber. As one

can reveal from the figure, λ_c continuously moves to the Stokes side with dose, with maximal shift observed for dose 5 (~75 nm relatively to its position in pristine state of the fiber): refer to the inset in **Figure 13**.

We may infer that the described phenomenon can be eventually explained by dose-dependent rise of BAC-related absorption in core region of BYP fiber, which, in accordance with Kramers-Kronig relations, ought to be accompanied by strong change (growth) of RI. Since darkening of the fiber in core area is measured by hundreds of dB/m around the cutoff wavelength (see **Figure 9**) while un-doped silica cladding is barely affected by irradiation (see **Figure 8**), we consider in the first approximation that core-cladding RI difference vs. dose is entirely defined by the changes arisen in the fiber core. λ_c-values, shown by violet symbols in the inset to **Figure 13**, can be recalculated into RI differences (δn), shown by orange symbols (see the right axis in the same plot). Seemingly, the found effect is pronounceable in BYP fiber due to weak RI difference (~4.3×10^{-3}) in its pristine state.

Let us gain insight into the bending loss issue by modeling of the waveguide properties of BYP fiber. Handling the measured RI profile of BYP fiber [11], we performed, using the software *Optiwave*, an analysis of the modes supported in its core region. An example of the results, obtained for the losses suffered by modes LP_{01} and LP_{11} modes, is demonstrated in **Figure 14**.

It is seen from **Figure 14** that the modeling results for bending loss for LP_{11} mode, viz., both the initial spectral position of cutoff wavelength in pristine BYP fiber and its movement with irradiation dose to longer wavelengths, qualitatively agree with the experiment (compare with **Figure 13**). Besides, the modeling results for bending loss for LP_{01} (fundamental) mode reveal a positive role of β-irradiation in the enhancement of transmittivity of this mode in the NIR. Also, our modeling allows one to understand one of the factors behind these trends, namely, better confinement of both LP_{01} and LP_{11} modes in the core area of the fiber with increasing irradiation dose [14].

To further cross-check the modeled and experimental circumstances of waveguiding and transmittivity in BYP fiber, **Figure 14** can be compared with **Figure 15** showing the transmission spectra of the fiber in pristine and irradiated states, coiled for diameter 30–40 cm. As seen from **Figure 15**, the pattern of WL transmittivity is a superposition of two basic trends, highlighted by the gray arrows: on the one hand, above ~1 μm, it is the rising of LP_{01} mode transmission due to enhanced confinement in the core region (compare with **Figure 14**), and, on the other hand, below ~1 μm, it is the worsening of transmission (merely due to IA).

The results shown above can be adopted, using the principles of modal interference, for making a simple BYP fiber-based sensor of ionizing radiation.

4. Conclusions

The general pattern of the changes in the basic optical characteristics of bismuth-doped yttrium-phosphosilicate fiber as the result of its irradiation by a beam of high-energy electrons is presented. Despite the dramatic rise of induced absorption in the fiber as the result of electron irradiation, we reveal its remarkable resistance, even at the highest doses of exposure, in terms of the emissive potential in VIS/NIR. The found laws of dose-dependent changes in the fiber's optical properties can be useful for dosimetry in harsh conditions, e.g., at a nuclear plant. It is separately emphasized for this type of bismuth-doped fiber the presence of a new effect, consisting in significant Stokes shift, experienced by its cutoff wavelength, proportional to the irradiation dose. As demonstrated, this effect, mainly associated

with an increase of the fiber's refractive index as the result of electron irradiation, can be also useful for the dosimetry purposes.

Acknowledgements

The authors are grateful to E. Sekiya and K. Saito (Japan), Y. Barmenkov and V. Minkovich (Mexico), S. Didenko, S. Legotin, and K. Tapero (Russian Federation), and J. Sahu (UK), for their valuable cooperation and helpful discussions. A. Kir'yanov acknowledges the support from the Increase Competitiveness Program of NUST "MISIS" of the Ministry of Education and Science (Russia) (Grant K3-2018-2023).

Author details

Alexander V. Kir'yanov[1,2*] and Arindam Halder[3,4]

1 Centro de Investigaciones en Optica, Leon, Mexico

2 National University of Science and Technology (MISIS), Moscow, Russia

3 Frontier Materials Laboratory, Toyota Technological Institute, Nagoya, Japan

4 Optoelectronics Research Center, University of Southampton, Southampton, UK

*Address all correspondence to: kiryanov@cio.mx

References

[1] Kir'yanov AV. Effects of electron irradiation upon absorptive and fluorescent properties of some doped optical fibers. In: Monteiro WA, editor. Radiation Effects in Materials. InTechOpen; 2016. ISBN 978-953-51-2418-4. DOI: 10.5772/61498

[2] Kir'yanov AV, Dvoyrin VV, Mashinsky VM, Il'ichev NN, Kozlova NS, Dianov EM. Influence of electron irradiation on optical properties of bismuth doped silica fibers. Optics Express. 2011;**19**:6599-6608

[3] Wen J, Liu W, Dong Y, Luo Y, Peng GD, Chen N, et al. Radiation-induced photoluminescence enhancement of Bi/Al-codoped silica optical fibers via atomic layer deposition. Optics Express. 2015;**23**:29004-29013

[4] Firstov SV, Khopin VF, Alyshev SV, Firstova EG, Riumkin KE, Melkumov MA, et al. Effect of gamma-irradiation on the optical properties of bismuth-doped germanosilicate fibers. Optical Materials Express. 2016;**6**:3303-3308

[5] Firstov SV, Khopin VF, Kharakhordin AV, Alyshev SV, Riumkin KE, Melkumov MA, et al. Radiation-induced absorption in bismuth-doped germanosilicate fibres. Quantum Electronics. 2017;**47**:1120-1124

[6] Kir'yanov AV, Barmenkov YO, Minkovich VP, Das S, Dutta D, Dhar A, et al. Effect of electron irradiation on the optical properties of bismuth doped hafnia-yttria-alumina-silicate fiber. Optical Materials Express. 2018;**8**:2550-2558

[7] Zhao Q, Luo Y, Hao Q, Peng GD. Electron beam irradiation and thermal-induced effects on the spectral properties of BAC-Al in Bi/Er codoped aluminosilicate fibers. Optical Materials Express. 2019;**9**:4287-4294

[8] Firstov SV, Khopin VF, Bufetov IA, Firstova EG, Guryanov AN, Dianov EM. Combined excitation-emission spectroscopy of bismuth active centers in optical fibers. Optics Express. 2011;**19**:19551-19561

[9] Obara K, Kakudate S, Oka K, Tada E, Morita Y, Sei M. Development of optical components for in-vessel viewing systems used for fusion experimental reactor. SPIE Proceedings. 1994;**2425**:115-122

[10] Paul SF, Goldstein JL, Durst RD, Fonck RJ. Effect of high-energy neutron flux on fiber optics in an active diagnostic on TFTR. The Review of Scientific Instruments. 1995;**66**:1252-1255

[11] Halder A, Kir'yanov AV, Sekiya EH, Saito K. Fabrication and characterization of bismuth-doped germano-silicate and phospho-silicate fibers for VIS/NIR applications. Optical Materials Express. 2019;**9**:1815-1825

[12] Kir'yanov AV, Halder A, Barmenkov YO, Sekiya EH, Saito K. Discussion on Raleigh scattering as a dominant loss factor in VIS/NIR in bismuth-doped silicate fibers [invited]. Optical Materials Express. 2019;**9**:2817-2827

[13] Halder A, Kir'yanov AV, Saito K. Broadband visible-to-NIR ASE from bismuth doped optical fibers: A window towards lasing. Japanese Journal of Applied Physics. 2019;**9**:120915

[14] Kir'yanov AV, Halder A, Sekiya E, Saito K, Barmenkov OA, Minkovich VP, et al. Impact of electron irradiation

upon optical properties of bismuth/yttria codoped phosphosilicate fiber. Optics & Laser Technology. 2020;**128**:106245

[15] Di Francesca D, Li Vecchi G, Girard S, Morana A, Reghioua I, Alessi A, et al. Qualification and calibration of single-mode phosphosilicate optical fiber for dosimetry at CERN. IEEE Journal of Lightwave Technology. 2019;**37**:4643-4649

[16] Di Francesca, D., Girard, S., Agnello, S., Alessi, A., Marchandella, C., Pailett, P., Querdane, Y., Kadi, Y., Brugger, M., Boukenter, A., "Combined temperature radiation effects and influence of drawing conditions on phosphorous-doped optical fibers," Physica Status Solidi A 216, art. 1800553 (2019)

[17] Girard S, Ouerdane Y, Marchandella C, Boukenter A, Quenard S, Authier N. Feasibility of radiation dosimetry with phosphorous-doped optical fibers in the ultraviolet and visible domain. Journal of Non-Crystalline Solids. 2011;**357**:1871-1874

[18] Girard S, Marchandella C, Morana A, Perisse J, Di Francesca D, Macé J-R, et al. Combined high dose and temperature radiation effects on multimode silica-based optical fibers. IEEE Transactions on Nuclear Science. 2013;**60**:4305-4313